JOURNAL OF GEOPHYSICAL RESEARCH, VOL. 103, NO. D24, PAGES 31,879–31,891, DECEMBER 27, 1998

Biomass burning aerosol size distribution and modeled optical properties

L. A. Remer and Y. J. Kaufman,
Laboratory for Atmospheres, NASA Goddard Space Flight Center, Greenbelt, Maryland

B. N. Holben,
Laboratory for Terrestrial Physics, NASA Goddard Space Flight Center, Greenbelt, Maryland

A. M. Thompson and D. McNamara
Laboratory for Atmospheres, NASA Goddard Space Flight Center, Greenbelt Maryland

Abstract. Satellite remote sensing of smoke aerosol and estimates of aerosol forcing of climate require knowledge of the aerosol optical properties. A smoke aerosol physical and optical model is developed from a database of over 800 volume size distributions inverted from sky radiance data measured by the AERONET radiometer network in Brazil over a 3-year period. The model represents total column, ambient conditions during the burning season in the Amazon Basin and cerrado region of Brazil. The mean volume size distributions are bimodal and can be represented by two lognormals. Accumulation mode modal radius is 0.13 ± 0.02 μm with $\sigma = 0.60 \pm 0.04$, and coarse-mode modal radius ranges from 6 to 40 μm, with a mean of 11.5 μm and $\sigma = 1.26 \pm 0.23$. The volume of each mode varies with optical thickness, causing the ratio of accumulation mode and coarse mode to vary as well, but the effect on the optical properties is negligible. Refractive index is taken to be $1.43–0.0035i$, and single scattering albedo is assumed to be 0.90, which is modeled with an external mixing of black carbon. The optical properties in the visible are dominated by the accumulation mode. Accumulation mode characteristics do not vary from year to year, from forest to cerrado region, with optical thickness or with precipitable water vapor. At one test location, accumulation mode characteristics do vary with air mass trajectory origin. The model is tested with independent data and can accurately predict the scattering phase function and path radiance in the backscattering direction that determines remote sensing properties and is responsible for scattering sunlight back to space.

1. Introduction

Smoke aerosol from biomass burning can cover one third of the South American continent during the burning season [*Prins et al.*, this issue] and wide areas of tropical Africa and the South Atlantic [*Herman et al.*, 1997]. It has been detected in the tropical South Pacific from Indonesian sources [*Folkins et al.*, 1997] and observed at higher latitudes as well [*Ferrare et al.*, 1990; *Stocks et al.*, 1996]. Because smoke aerosol is a global phenomenon, it is suspected of playing a role in Earth's global energy balance [*Intergovernmental Panel on Climate Change* (IPCC), 1996]. Smoke aerosol absorbs and scatters solar radiation and therefore may act as a negative direct forcing by scattering solar radiation back to space [*Penner et al.*, 1992; *Hobbs et al.*, 1997]. Smoke may also act through modifications to cloud microphysics to increase cloud albedo and create an indirect radiative forcing [*Twomey*, 1977b; *Twomey et al.*, 1984; *Kaufman and Nakajima*, 1993; *Kaufman and Fraser*, 1997]. Quantification of these possible radiative forcing pathways and narrowing the uncertainties expressed in the IPCC report are dependent on estimations of smoke optical and physical properties. *Hobbs et al.* [1997] show that updating the optical parameters in Penner's model results in a much reduced global forcing.

Previous attempts to create generalized aerosol models did not include smoke aerosol [*Shettle and Fenn*, 1979; *Lenoble and Brogniez*, 1984] due to lack of measurements. Climate modelers and satellite remote sensing scientists have relied on compilations of the results of individual field campaigns and surface-based in situ sampling stations. Southern African Fire-Atmosphere Research Initiative (SAFARI) [*Le Canut et al.*, 1996a, b; *Andreae et al.*, 1996], Transport and Atmospheric Chemistry Near the Equatorial Atlantic (TRACE A) [*Anderson et al.*, 1996], and Smoke, Clouds, and Radiation–Brazil (SCAR-B) [*Reid et al.*, this issue] have provided samples of tropical biomass burning aerosol size distributions from aircraft measurements. *Radke et al.* [1991] present aerosol characteristics measured from aircraft in North America. Aircraft measurements permit resolution of the vertical profiles of aerosol characteristics but, in turn, must be integrated to achieve total column values. Aerosol above or below the vertical profile is either estimated or ignored [*Ross et al.*, this issue]. Aircraft measurements are sparse in time. For example, *Le Canut et al.* [1996a] base their results on 48 profiles collected on only 10 days. In contrast, ground-based in situ sampling can be maintained over a long time period [*Maenhaut et*

Paper number 98JD00271.
0148-0227/98/98JD-00271$09.00

al., 1996; P. Artaxo et al., unpublished data, 1997]. However, as *Le Canut et al.* [1996a] show, there does exist a vertical gradient to smoke aerosol particle size. Thus ground sampling may be biased when applied to total column aerosol. Both ground-based and airborne in situ measurements alter the aerosol before measuring [*Remer et al.*, 1997] and are affected by the size-influenced sampling efficiency of each in situ system [*Huebert et al.*, 1990]. Because some in situ measurements dry the aerosol, ambient size distributions are achieved only after a humidification factor is applied [*Kotchenruther and Hobbs*, this issue].

Automatic Sun/sky scanning spectral radiometers have been used successfully to retrieve total column, ambient spectral aerosol optical thickness, and volume size distribution [*Holben et al.*, 1998]. These instruments, manufactured by Cimel, work every day, sunrise to sunset, week after week, for the duration of the burning season. A network of ground-based Sun/sky radiometers has been deployed in the Amazon Basin of Brazil during the burning seasons from 1993 to 1995 [*Holben et al.*, 1996a]. The radiometers use Sun measurements at 340, 440, 670, 870, 940, and 1020 nm to derive spectral optical thickness and total column precipitable water vapor. Certain instruments have been upgraded to include measurements at 380 and 500 nm. The instruments also invert sky measurements at 440, 670, 870, and 1020 nm to obtain volume size distribution and phase function. The sky measurements are taken in the principal plane of the Sun during midday and in the Sun's almucantar (a plane defined by a fixed view elevation angle that includes the Sun) when the Sun is low in the sky.

A similar network of these instruments located in the United States was used to develop a dynamical aerosol model for urban/industrial aerosol [*Remer et al.*, 1996; *Remer and Kaufman*, 1998]. The same technique was applied to the 1993 data of two Brazilian stations, and a preliminary model of smoke optical properties was constructed [*Remer et al.*, 1996]. In this study we construct an optical model using the full 3 year data set that includes data from 13 stations. The additional data permit calculation of the uncertainties in the physical and optical parameters of the smoke model. The model is tested against similar data measured in Cuiabá during the 1995 burning season that was purposely withheld from the original database in order to achieve an independent testbed. Sensitivities to various values of refractive index and single scattering albedo are explored. The variability of smoke properties in Brazil is analyzed in terms of smoke transport, and the use of precipitable water vapor as a tracer for different smoke properties is investigated.

2. Data

During the burning seasons of 1993–1995 a network of automatic Sun/sky scanning spectral radiometers was deployed in the Amazon Basin as part of the Aerosol Robotic Network (AERONET) global network and in conjunction with the SCAR-B experiment [*Kaufman et al.*, this issue; *Holben et al.*, 1996a]. Instruments were located at 13 semipermanent sites. Not every site was instrumented each year. The radiometers measure sky radiance in the Sun's almucantar once per hour in the morning and late afternoon, when the Sun's zenith angle is greater than 60°. This procedure provides at most six almucantar measurements per station per day. However, the almucantars are checked for symmetry of the sky radiance on either side of the Sun, and asymmetrical almucantars (difference >10%) are discarded. Asymmetry occurs due to nonhomogeneous atmospheric conditions. Cloud conditions are discarded as well. Altogether, over 800 symmetrical almucantars were retrieved for the period of deployment and used to construct the model. In addition, 27 retrieved size distributions from the Cuiabá station in 1995 were set aside to be used in the testing process.

The sky radiances from each symmetrical almucantar are inverted to achieve aerosol volume distribution [*Nakajima et al.*, 1983, 1986]. Sensitivity tests of the inversion process show average errors in the 0.10–8 μm radius range of less than 10%, corresponding to uncertainties in calibration, stray light, assumptions of real and imaginery refractive index, and surface albedo [*Kaufman et al.*, 1994]. The inversion is most sensitive to errors in scattering angle, which result in overpredictions of coarse-mode volume of 40% [*Kaufman et al.*, 1994]. The inversion of volume in the radius range below 0.10 μm diverges from the true distribution because the inversion algorithm assumes that beyond the size limits of the inversion (0.07 and 9 μm) the particle volume is zero. This assumption affects the resulting volume distribution by artificially increasing volume at the size limits of the inversion in order to compensate for the arbitrary and unphysically low volume just beyond the limits. These problems are isolated to the radius ranges near the edges of the inversion range. We correct the [*Nakajima et al.*, 1983, 1986] inversion at the small-particle end by assuming these particles can be represented by a single lognormal distribution and by conserving the optical properties of the original inversion [*Remer et al.*, 1997; *Remer and Kaufman*, 1998]. Note that although the small-particle range has been corrected for the inversion's overprediction, the large-particle range has not. The same artifact that affects the small particles also affects the large particles, and so the exact size of the coarse mode's modal radius may be physically incorrect. The correction procedure has not been applied to the large-particle end due to possible contamination by stray light in the instrument and the relative insensitivity of the optical properties in the visible region to coarse-mode particles. The 800 volume size distributions were divided into cerrado stations and forest stations, then sorted and ordered according to increasing aerosol optical thickness at 670 nm. The cerrado and forest subsets were analyzed separately. Most of the data (~625 size distributions) were retrieved from the cerrado stations, and the remainder from forest stations. Each 10–60 size distributions were averaged to give the mean size distribution for a particular aerosol optical thickness [*Kaufman and Holben*, 1996]. The curves are plotted in Figure 1.

The smoke aerosol appears to be bimodal with an accumulation mode peaking at 0.12–0.16 μm and a coarse mode at roughly 3–10 μm. In contrast, a trimodal volume size distribution (r_m = 0.13–0.15, 0.50 and >1.5 μm) was found in aircraft measurements during TRACE A [*Anderson et al.*, 1996] and SAFARI [*Le Canut et al.*, 1996a, b]. However, the mode at 0.50 μm is small and difficult to distinguish. Ground-based sampling suggests a bimodal distribution with modes peaking at approximately 0.15 and 1.5 μm, respectively (P. Artaxo et al., unpublished data, 1997). Other measurements of smoke also find an accumulation mode with mean volume radius in the 0.12–0.17 μm range [*Radke et al.*, 1991; *Andreae et al.*, 1994; *Ji et al.*, 1996; *Reid et al.*, this issue]. Figure 1 shows that as aerosol optical thickness increases, aerosol volume increases in both modes in the cerrado, but mainly for the accumulation mode in the forest. However, the mean radius size of

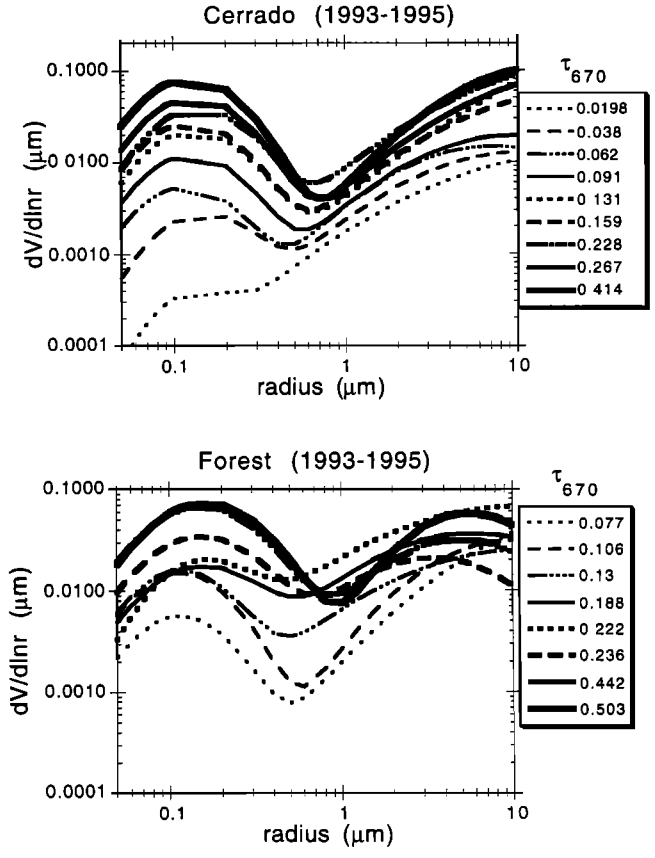

Figure 1. Volume size distributions for several aerosol optical thicknesses at 670 nm for the cerrado stations (top) and forest stations (bottom). Each curve represents a mean of 10–60 individual size distribution retrievals. Size distributions corrected at small particle end for overprediction of volume by inversion method. Not every curve calculated is plotted.

each mode remains more or less the same. This is in contrast to urban/industrial aerosol measured in the mid-Atlantic region of the United States that show a distinctive increase in accumulation mode radius size with increasing aerosol optical thickness [*Remer et al.*, 1996, 1997; *Remer and Kaufman*, 1998].

The reasons for the difference between smoke and urban/industrial aerosol are complex. Urban/industrial aerosol is affected by gas phase oxidation that generates particles, cloud processing that creates most of the mass of the dry particles [*Hoppel et al.*, 1990; *Kaufman and Tanré*, 1994], and because of a large humidification factor, swelling from humidity. In contrast, smoke has a much smaller humidification factor, and so particle growth from water intake is much smaller [*Kotchenruther and Hobbs*, this issue]. Also the smoke aging process is a shorter lived phenomenon that results in increases of mass of roughly 20–50%, at most a 15% increase in radius [*Reid et al.*, this issue]. However, most of the aging takes place in dense smoke plumes and is finished before the sunphotometer measures a well-mixed homogeneous sky and before the smoke spreads over a wide enough area to have a climatic effect.

Figure 2 shows the error bars calculated from the standard deviation of the size distributions about the mean curves for four selected curves of Figure 1. The variations in size distributions are large at the small- and large-particle ends due to uncertainties in the inversion at the end points. The variation is also large at 0.55 μm. This may be due to the elevated stratospheric aerosol concentrations caused by the Mount Pinatubo eruption of 1991 that were still evident in 1993. Although the stratospheric mode was fitted by a lognormal [*Remer et al.*, 1996] and subtracted from the 1993 data in the database, some large variation in the size distributions have remained. Another possibility is that the mode at 0.50 μm observed during TRACE A and SAFARI may be intermittent in the AERONET database. Overall, there is minimal deviation from the mean curve in the 0.1–0.3 and 1.0–5.0 μm ranges that define the accumulation and coarse modes, respectively.

3. Aerosol Model

We assume that each of the modes in Figure 1 can be represented by a lognormal given by

$$\frac{dV}{d\ln r} = \frac{V_0}{\sigma(2\pi)^{1/2}} \exp\left(-\frac{[\ln (r/r_m)]^2}{2\sigma^2}\right) \quad (1)$$

where $dV/d\ln r$ is the volume distribution, V_0 is the column volume of the particles per cross section of atmospheric column, r is the radius, r_m is the modal radius, and σ is the standard deviation of the natural logarithm of the radius. The sum of the modes will reproduce the original, corrected volume distribution curve for each particular optical thickness. Another way of expressing the modes is with a number distribution defined as

$$\frac{dN}{d\ln r} = \frac{N_0}{\sigma(2\pi)^{1/2}} \exp\left(-\frac{[\ln (r/r_g)]^2}{2\sigma^2}\right) \quad (2)$$

where N_0 is the number of particles per cross section of the atmospheric column (cm^{-2}), σ is the same as in (1), and r_g is the modal radius of the number distribution. The parameter r_g is related to r_m by

$$r_g = r_m \exp(-3\sigma^2) \quad (3)$$

V_0 of (1) is related to N_0 by

$$V_0 = \frac{4N_0\pi}{3} \exp\left(\frac{9\sigma^2}{2}\right) r_m^3 \quad (4)$$

Each of the mean curves in Figure 1 is fit to (1), and the parameters r_m, σ, and V_0 are calculated. These values are given in Table 1 and depicted graphically in Figures 3 and 4. Also shown in Table 1 are the values calculated in the preliminary analysis of the 1993 cerrado stations [*Remer et al.*, 1996].

3.1. Accumulation Mode

The accumulation mode volume V_0 increases with increasing aerosol optical thickness at nearly the same rate for both the cerrado and forest models. The accumulation mode particle size r_m shows some variation with optical thickness for the clearest conditions, which may be due to atypical aerosol or meteorological conditions, then stabilizes at 0.145 μm. The cerrado smoke has a slightly smaller r_m that does not vary with optical thickness. The cerrado r_m is remarkably consistent within each data set and between the 1993–1995 database and the preliminary 1993-only data set. Both the cerrado and forest values fall within the range of smoke values reported in the literature [*Anderson et al.*, 1996; *Le Canut et al.*, 1996a, b; *Radke et al.*, 1991; *Andreae et al.*, 1994; *Ji et al.*, 1996; *Reid et al.*, this issue]. On the other hand, accumulation mode σ has increased from 0.50 in 1993 to 0.60 in the full 3-year data set. The

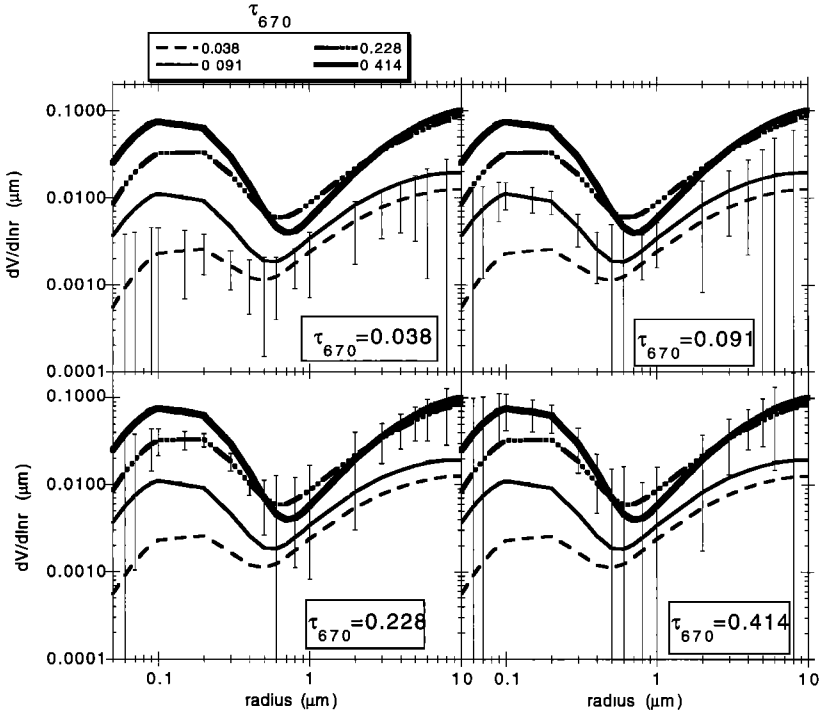

Figure 2. Four selected curves of Figure 1 cerrado data shown plotted with error bars representing the standard deviation of the individual retrievals about the mean curve. The mean curve bracketed by error bars in each panel is indicated by the optical thickness value.

width of the accumulation mode as represented by σ may be affected by the subtraction of the stratospheric component in the 1993 data. It was previously noted that there is an increase in uncertainty in the volume size distributions in the 0.5–0.6 μm range (Figure 2). This radius range corresponds to the upper tail of the accumulation mode and may affect the calculation of σ. Both the old and new values of σ fall within the range of values (σ = 0.40–0.60) measured by *Reid et al.* [this issue]. Smoke properties at the forest stations tend to be more variable than at the cerrado stations.

3.2. Coarse Mode

The coarse-mode volume V_0 increases with optical thickness in the cerrado data set but varies randomly in the forest data set. The other coarse-mode parameters do not exhibit a steady increase with optical thickness and are fixed at their mean value. The variation in coarse-mode parameters is larger than the variation in the remarkably consistent accumulation mode parameters. The coarse-mode model has a large uncertainty because the coarse mode is plagued by possible sensitivity to

Table 1. Lognormal Parameters and Uncertainties for the Cerrado and Forest Sites and From the Original Analysis of the 1993 Cerrado Sites

	Cerrado	Forest	1993
Accumulation			
V_0, μm	$-0.0089 + 0.31\tau_{670}$	$-0.017 + 0.30\tau_{670}$	0–0.31
r_m, μm	0.132 ± 0.014	$0.074 + 0.36\tau_{670}$ ($\tau_{670} < 0.20$) 0.145 ± 0.025 ($\tau_{670} \geq 0.20$)	0.13
σ	0.60 ± 0.04	0.60 ± 0.09	0.50
Coarse			
V_0, μm	$0.035 + 0.81\tau_{670}$	0.15 ± 0.11	0.04–0.27
r_m, μm	6–40 (mean 11.5)	2–30 (mean 9.0)	6–20
σ	1.26 ± 0.23	1.20 ± 0.30	0.7–1.2
ECCN/τ (0.3%), μm^{-2}	123 ± 33		
ECCN/τ (1%), μm^{-2}	162 ± 60		
α_{av}, $\mu m^2/\mu m^3$	3.2 ± 0.1		

Uncertainties represent standard deviations. Volumes are in units of volume per unit area. Also listed are calculations of effective CCN (ECCN) per unit optical thickness per unit area based on the critical radii at 0.3% and 1% supersaturations, and the accumulation mode volume scattering efficiency at 670 nm (α_{av}).

stray light in the instrument and also to the problems with the inversion at the upper radius bound of the inversion range. Furthermore, we expect the larger aerosol to have shorter lifetimes and be more variable in space and time. Thus we do not place much emphasis on the model for the coarse mode. In the biomass burning regime the optical properties are dominated by smaller particles. For example, for $\tau_{670} \geq 0.30$ the accumulation mode accounts for roughly 95% of the total extinction. At $\tau_{670} < 0.30$ the coarse mode gradually makes a greater contribution to total extinction, so that in very clean conditions ($\tau_{670} = 0.05$) the coarse mode contributes as much as 30% toward the total extinction. Still, in most smoky conditions the accumulation mode dominates, and uncertainties in the coarse-mode model are relatively unimportant.

3.3. Volume Scattering Efficiency and Effective Cloud Condensation Nuclei

The smoke aerosol accumulation mode ($r < 0.5$ μm) is the dominant mode describing the optical properties. The volume scattering efficiency of the accumulation mode, α_{av}, describes the ratio between the scattering cross section of the particles and their volume. A high scattering efficiency means a high scattering ability for a given aerosol mass. The parameter α_{av} is calculated and shown in Table 1 for the cerrado model. The mass scattering efficiency, α_{am} is given by α_{av} divided by the appropriate aerosol density. A density of 1.35 g/cm^3, measured by *Reid and Hobbs* [this issue], yields $\alpha_{am} = 2.4$ m^2/g at 670 nm. *Reid et al.* [this issue] measure a similar value of $\alpha_{am} = 1.8$ m^2/g at 700 nm.

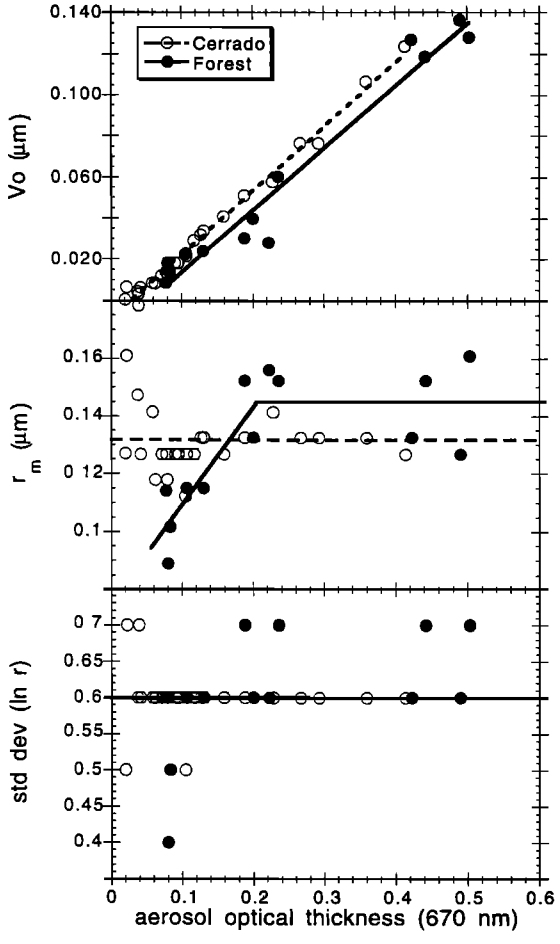

Figure 3. Accumulation mode lognormal parameters plotted as function of aerosol optical thickness for cerrado and forest stations.

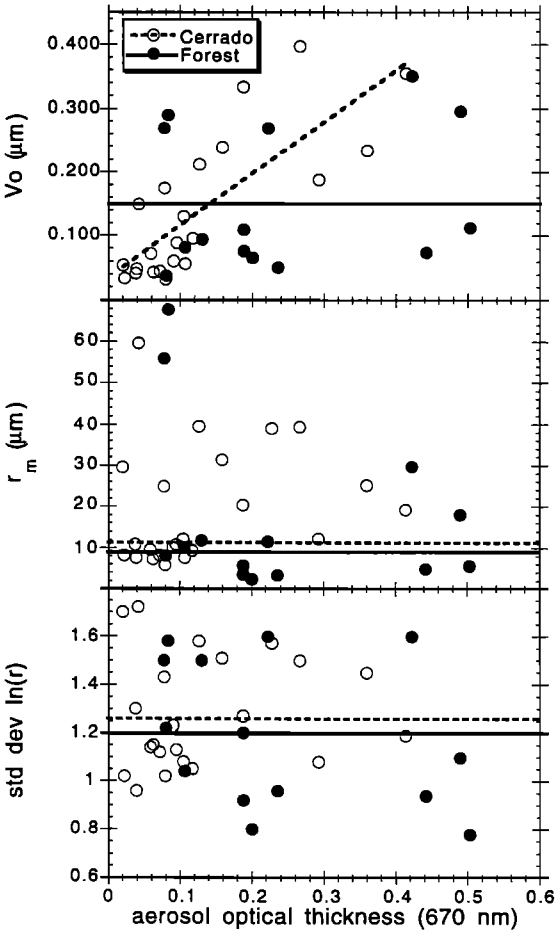

Figure 4. Coarse mode lognormal parameters plotted as function of aerosol optical thickness for cerrado and forest stations.

Satellite estimates of the effect of aerosol on cloud properties [*Kaufman and Fraser*, 1997] are based on the assumption that the satellite-derived optical thickness is proportional to the number of potential cloud condensation neuclei (CCNs) (particles larger than a given activation radius). This proportionality can be reduced due to instability of the aerosol size distribution and the corresponding ratio between the aerosol volume and number of particles. Our data show that for smoke the increase in optical thickness is due to an increase of total volume and number of the accumulation mode aerosol, not due to a shift of aerosol size into a more optically effective range. It is thus expected that optical thickness will also be proportional to the number of effective CCNs. Q. Ji et al. (Ground-based measurements of aerosol characteristics in biomass burning and industrial pollution episodes, submitted to *Journal of Geophysical Research*, 1997; hereinafter referred to as submitted paper) confirm the relationship between aerosol number and volume; they also show that the aerosol is hygroscopic at high humidities. These data imply that an effective CCN (ECCN) per unit optical thickness can be calculated based on the critical radius as defined by

Table 2. Optical Parameters

	440 nm	670 nm	870 nm	1020 nm
g	0.65 ± 0.04	0.57 ± 0.06	0.50 ± 0.06	0.45 ± 0.07
β	0.24 ± 0.02	0.27 ± 0.02	0.31 ± 0.02	0.32 ± 0.03
ω_0	0.90	0.90	0.90	0.90

Asymmetry factor g, backscattering coefficient β [after *Wiscombe and Grams*, 1976], and single scattering albedo ω_0 calculated from the cerrado model of Table 1 for four wavelengths. Uncertainties are calculated from the uncertainties of the cerrado model and encompass the variation exhibited by the other two models (see Figure 6). The single scattering albedo is an estimate based on the work by *Kaufman et al.* [1992], not a calculation. The estimate was tested against measured sky radiance (see Figure 8).

$$r_c = 0.0145 S_c^{-2/3} \tag{5}$$

where r_c is the critical radius in microns and S_c is the supersaturation [*Twomey*, 1977]. Data measured during SCAR-B show that (5) holds to within the experimental uncertainties (Q. Ji et al., submitted paper, 1997). Calculations are made for $S_c = 0.3\%$ and 1% for the size distributions of the cerrado model and shown in Table 1. Note that even though *Kotchenruther and Hobbs* [this issue] found that the smoke humidification factors are small (1.25–1.5), Q. Ji et al (submitted paper, 1997) found the aerosol to behave as efficient CCN in agreement with previous studies [*Hobbs and Radke*, 1969; *Radke et al.*, 1991; *Hudson et al.*, 1991; *Rodgers et al.*, 1991].

4. Optical Properties

The optical properties of the smoke aerosol are calculated using the Mie code of *Dave and Gazdag* [1970]. We assume the aerosol to be spherical, which is generally true for smoldering fires and less so for flaming fires [*Martins et al.*, this issue]. In all the calculations, we take the complex refractive index to be $1.43–0.0035i$. This assumes a minimal amount of internally mixed black carbon in the aerosol. The single scattering albedo ω_0 for this complex refractive index is 0.97. Additional absorption is simulated with an external mixing of black carbon that brings ω_0 down to 0.90. *Hobbs et al.* [1997] use $\omega_0 = 0.88$ in their calculation. Section 5 examines the sensitivity of the model to these assumptions of refractive index and absorption. Table 2 shows the values of asymmetry parameter g and backscattering coefficient β calculated from the model.

The spectral dependence of the extinction coefficient of the models is shown in Figure 5. The extinction coefficient has been normalized by values at 550 nm. The curves represent the three models listed in Table 1, each for a low and high optical thickness. Optical properties remain mostly constant for all optical thicknesses for the cerrado model. All five model–optical thickness combinations show very similar spectral dependence. The angstrom coefficient is defined as α in the equation

$$\tau = A\lambda^{-\alpha} \tag{6}$$

Angstrom coefficients calculated from these curves using wavelengths between 380 and 1020 nm range from 2.1 to 2.4, with the cerrado model falling about midway in this range. Also shown in Figure 5 is the spectral dependence of the extinction optical thickness obtained from the direct Sun measurements. The Sun data curve represents the mean of approximately 100 individual observations with $\tau_{670} \sim 0.40$ from stations located throughout the cerrado region. These data are typical of any grouping of Sun data in smoky conditions. The Sun data show less spectral dependence ($\alpha = 1.82 \pm 0.19$) than the model data derived from sky radiance observations but do overlap the model data within the ranges of uncertainty. By any measurement, the smoke shows a much stronger wavelength dependence than urban/industrial aerosol, which has an angstrom exponent of around 1.5 for $\tau > 0.2$ [*Remer and Kaufman*, 1998].

The phase function calculated at two wavelengths using the model parameters is shown in Figure 6. The five curves represent the same model-optical thickness combinations of Figure 5. The error bars calculated for the cerrado model at 670 nm and plotted in the insert panel show that the variation between models lies within the variation expected of any individual model. Thus we conclude that the models listed in Table 1 are not significantly different from each other. There appears to be a very strong consistency in the smoke aerosol from region to region, from year to year, and for various amounts of smoke loading. Any of the models could be chosen to represent the smoke aerosol. In subsequent analyses done for this paper, we will employ the cerrado model because its optical properties fall midway among the different models.

Figure 7 shows the mean fractional error of the cerrado model phase function as a function of scattering angle for two wavelengths and is based on the standard deviation of r_m and σ expressed in Table 1. Despite the consistency in mean smoke aerosol size distribution and optical properties, there is variability about the mean. On a day-to-day basis, errors in backscattering phase function of within 20–30% can be expected 2/3 of the time, while even greater errors can be expected 1/3 of the time.

5. Testing the Model

The model is tested in two ways. First, the model was derived from volume size distributions that were retrieved from sky

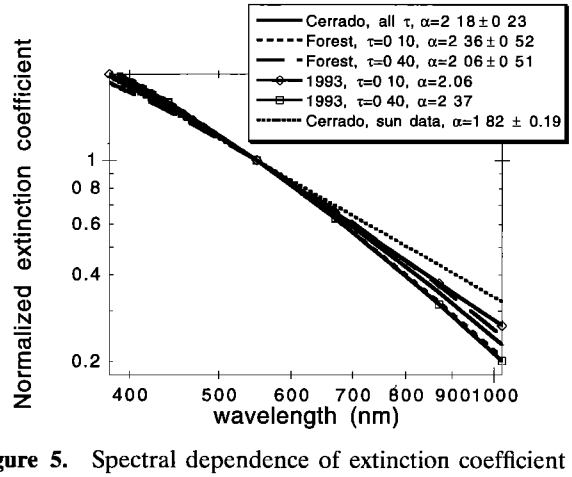

Figure 5. Spectral dependence of extinction coefficient calculated for cerrado version of the model and for forest and 1993 versions of the model for low and high values of optical thickness. Dotted line shows spectral dependence of extinction optical thickness calculated from Sun observations of the radiometers. Extinction coefficients are normalized by value at 550 nm. Also shown are calculated values of mean angström coeficient α and uncertainties due to uncertainties of lognormal parameters expressed in Table 1. Uncertainty of Sun data is calculated from the database. Uncertainties are unavailable from original 1993 derivation.

radiance data in the first 40° from the Sun. Thus the sky radiance data measured by the radiometers in the backscattering direction provide an independent database to test model predictions. Second, the 1995 Cuiabá data were excluded from the original database in order to retain additional independent data for test purposes. We use the model to predict smoke optical properties, specifically, phase function, and to compare these predictions to actual conditions measured at Cuiabá in 1995.

5.1. Prediction of Backscattered Sky Radiance

Figure 8 shows the observed downwelling normalized path radiance for a solar zenith angle of 60° and a scattering angle of 120°. Over 300 observations were made at this geometry. Also plotted are curves calculated from the *Dave and Gazdag* [1970] radiative transfer code using the cerrado size distribution model described above. The *Dave and Gazdag* [1970] code is a full radiative transfer code that takes into account multiple scattering, although it does not include polarization. The panels on the left show the full range of optical thickness values encountered. The panels on the right expand the axes to show more clearly the lower optical thickness range. The plots depict the model sensitivity to different assumptions of refractive index and absorption. The observations are the same in each of the plots. The wavelength of 670 nm is chosen because it has remote sensing applications (channel 1 on a very high resolution radiometer (AVHRR)) and because the standard wavelength representing the solar maximum (550 nm) is not available on the sky radiometer (440, 670, 870, and 1020 nm).

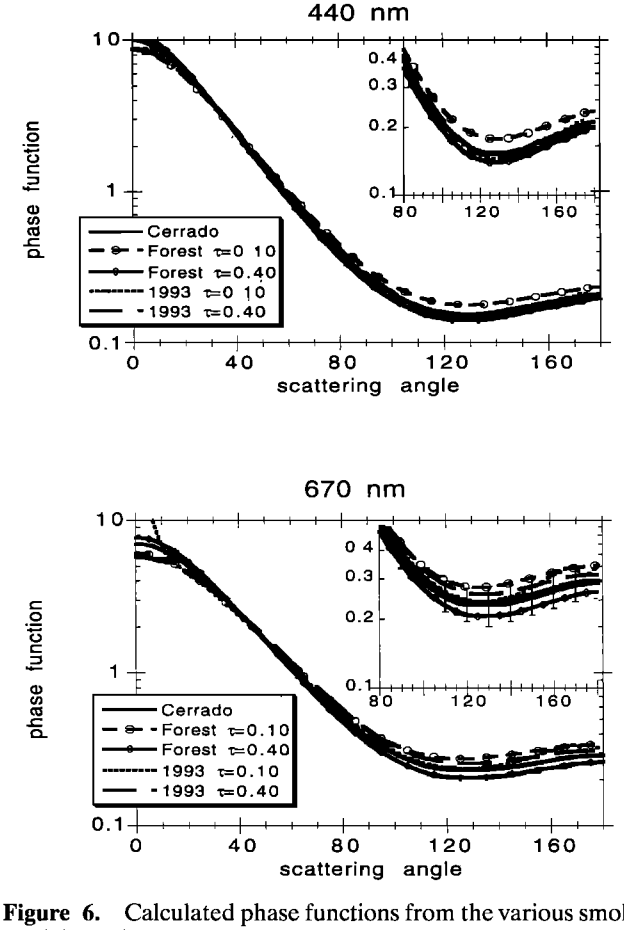

Figure 6. Calculated phase functions from the various smoke models at different optical thicknesses. Top panel shows 440 nm, and bottom panel 670 nm. Insert in each plot shows enlargement of backscattering portion of the phase function. The 670 nm insert shows errors bars on the cerrado curve (solid curve) representing the uncertainty in the phase function resulting from the uncertainty in the lognormal parameters of Table 1.

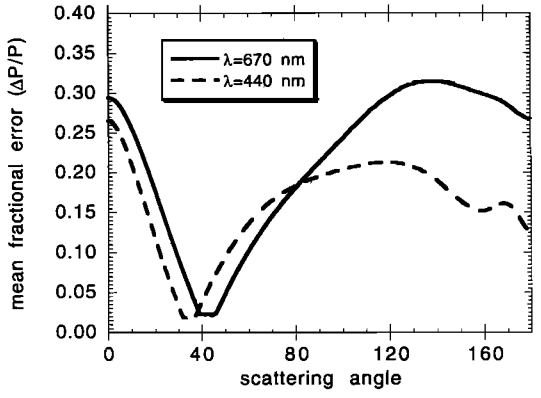

Figure 7. Mean fractional error in predicting the phase function at 670 and 440 nm based on the uncertainty in calculating the mean size distribution parameters for the cerrado model of Table 1. Error represents one standard deviation from mean parameters.

The top panels of Figure 8 show sensitivity to variations in the real part of the refractive index n_r. From this analysis, values of n_r from 1.35 to 1.6 seem to fit the data. This suggests that backscattering radiance is not sensitive to the values of n_r. The value of $n_r = 1.43$ used in our calculations of aerosol optical properties falls within the range of scatter of the data. Originally, 1.43 was chosen to represent the result of mixing a dry, yet hygroscopic, smoke particle ($n_r = 1.55$) with water ($n_r = 1.33$). *Yamasoe et al.* [this issue] make a more careful analysis to determine the refractive index of smoke aerosol. They find higher values for the real part of the refractive index ($n_r \sim 1.55$) than the value we use, corresponding to the low humidification factor found by *Kotchenruther and Hobbs* [this issue].

The bottom panels of Figure 8 show the sensitivity of the model to variations in single scattering albedo. The complex refractive index was held constant at $1.43-0.0035i$, while black carbon was added in an external mixture. We see that backscattering radiance is sensitive to single scattering albedo. The value used in the calculations of section 4, 0.90, is representative of mean conditions throughout the full range of optical thicknesses. Lower values of ω_0 measured in situ [*Reid et al.*, this issue] do not fit the sky radiance data at moderate to high optical thicknesses. The precise determination of the refractive index and single scattering albedo is best left to other analyses [*Yamasoe et al.*, this issue; *Eck et al.*, this issue; *Holben et al.*, 1996b; *Reid et al.*, this issue]. The above analyses were done simply to show that the size distribution model developed from sky radiance in the first 40° from the Sun can successfully predict the sky radiance in the backscattering direction given reasonable values of index of refraction and single scattering albedo.

5.2. Prediction of Optical Properties at Cuiabá

The 1995 data from the Cuiabá site were withheld from the original database used to construct the aerosol models of Table

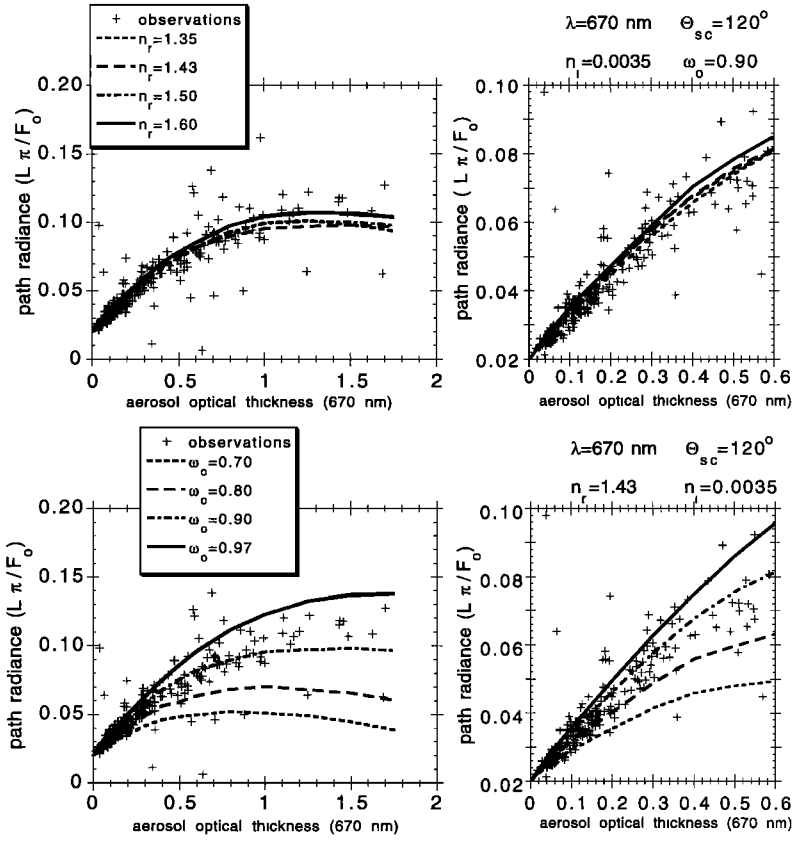

Figure 8. Normalized downwelling path radiance at 670 nm for a scattering angle of 120° and a solar zenith angle of 60° as a function of aerosol optical thickness at 670 nm. Crosses indicate individual observations by the AERONET radiometers. The curves represent values calculated from the cerrado model in Table 1. The top panels show the sensitivity of the model to various values of the real part of the refractive index (n_r) with single scattering albedo held constant at 0.90 and the imaginary part of the refractive index held constant at 0.0035. The bottom panels show the sensitivity of the model to various values of single scattering albedo (ω_0) with the complex refractive index held constant at $1.43-0.0035i$. The left panels show the full range of measured values. The right panels show values for $\tau \leq 0.60$ on an expanded axis.

1. There were 27 almucantar inversions achieved from August 22 through November 14, 1995. These data represent aerosol conditions ranging from optical thicknesses at 670 nm of 0.09–1.11. The retrieved phase functions from the Cuiabá data set were sorted according to aerosol optical thickness and averaged for every three size distributions. Figure 9 shows the model phase function plotted on the same graph as the phase functions observed at Cuiabá during this 1995 period. The model does an excellent job of predicting the phase function at Cuiabá, especially at the higher optical thicknesses. There appear to be systematic discrepancies between Cuiabá data and the model at small scattering angles. These indicate a poor representation of the coarse mode in the model. However, the overall good agreement in phase functions indicates an accurate representation of the more important accumulation mode.

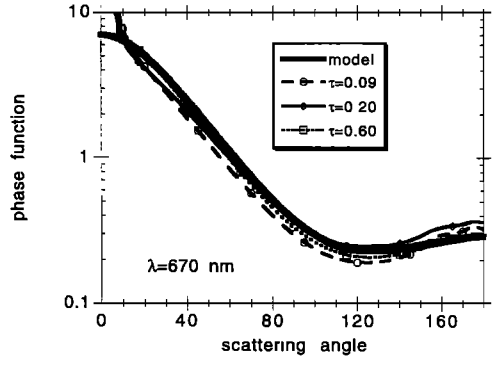

Figure 9. Phase function of the model calculated with cerrado model parameters plotted with phase functions calculated from data collected at Cuiabá in 1995 at different aerosol loadings.

6. Variability of Smoke Aerosol in Brazil

The results from the modeling effort, above, suggest that all smoke is the same and all smoke can be predicted (within the calculated errors) from a model based on mean properties of a smoke database. Other studies suggest otherwise. In situ samples and scanning electron microscope analysis from smoke plumes show that characteristics of smoke particles are very dependent on flaming/smoldering ratios of the fire or from the type of fuel burned [*Martins et al.*, 1996, this issue]. It is possible these differences maintain themselves only through a short lifetime and that the widespread regional haze measured by the AERONET instruments used in the modeling is a well-aged, mixed, much more uniform aerosol. Still, there is vari-

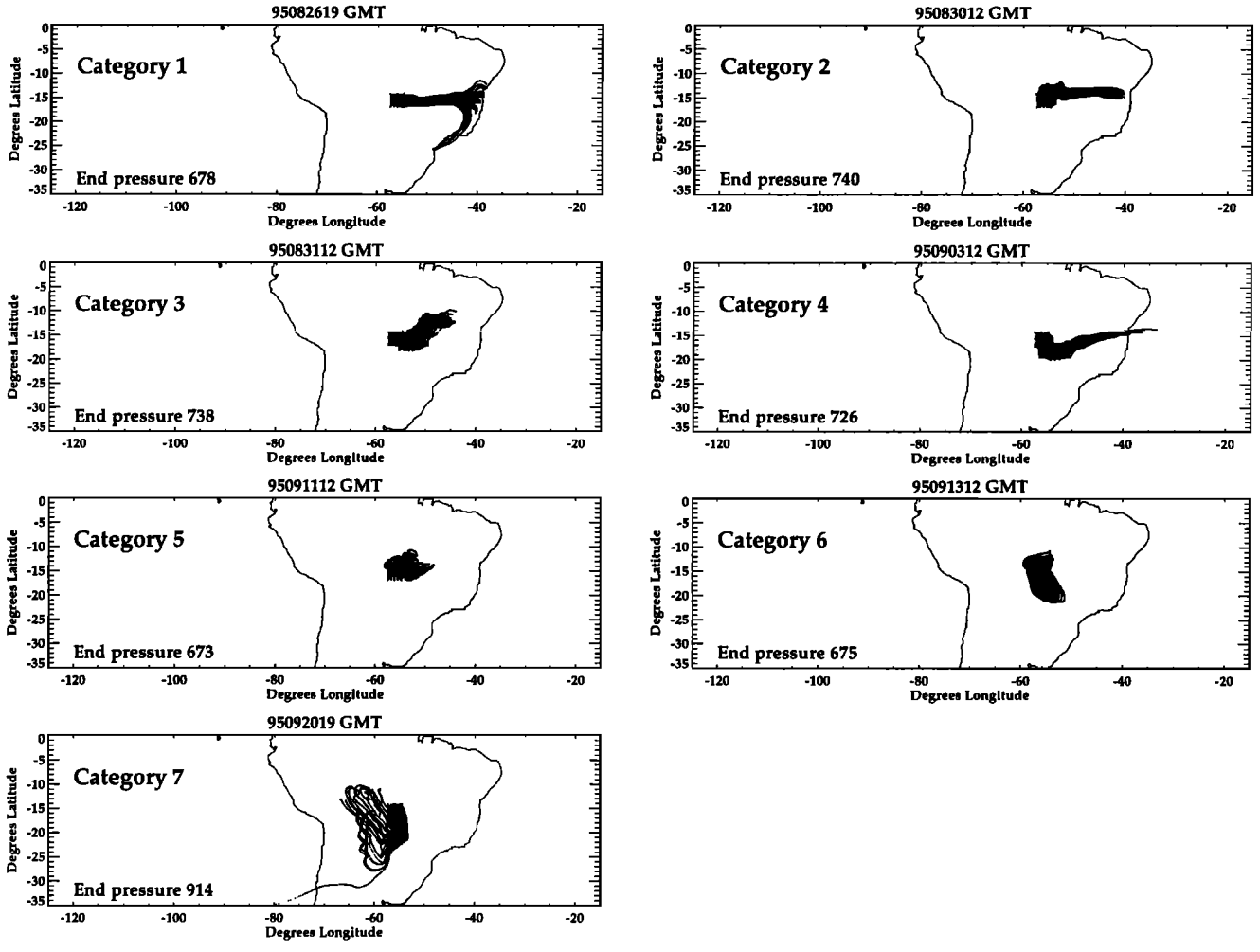

Figure 10. One example of each category of back trajectories from Cuiabá at the 800 mbar level.

ability in the regional haze. So far, this variability has been treated as random error. Now we take a closer look at the variability of the regional haze measured at Cuiabá during the period August 26 to October 1, 1995. Back trajectories are calculated to separate the database into different categories dependent on the origin of the boundary layer air mass. We then investigate the different properties of the aerosol measured by the AERONET instrument to determine whether or not there are systematic variations in the aerosol optical properties.

6.1. Back Trajectories From Cuiabá

Trajectories were run in 5 × 5 clusters within a 2.5° by 2.5° grid around Cuiabá using the NASA GSFC isentropic trajectory model. Three levels were resolved: 300, 600, and 800 mbar. The model allows air parcels to start at specific pressure levels and multiple start times [*Schoeberl et al.*, 1993; *Schoeberl and Sparling*, 1995; *Pickering et al.*, 1996]. National Center Environmental Prediction (NCEP) analyses were used to drive the model. The 37 days of calculated back trajectories were

Table 3. Seven Trajectory and Air Mass Origin Categories

Category	Definition	Days	τ	$\alpha_{870/440}$	P_w
1	E, strong descent	4	0.47	−1.90	1.70
2	ENE, descent	4	0.79	−1.81	2.90
3	NE, descent, stagnant	9	0.87	−1.72	3.25
4	ESE, descent	8	0.58	−1.64	2.53
5	Local, strong descent	3	0.70	−1.75	2.78
6	SE, strong descent	2	1.00	−1.55	4.10
7	S, W, ascent	7	0.68	−1.61	3.53

Shown are the number of days falling into each category, the mean aerosol optical thickness at 670 nm (τ), wavelength exponent ($\alpha_{870/440}$), and precipitable water vapor (P_w) in each category observed at Cuiabá on the day of the start time of the back trajectory.

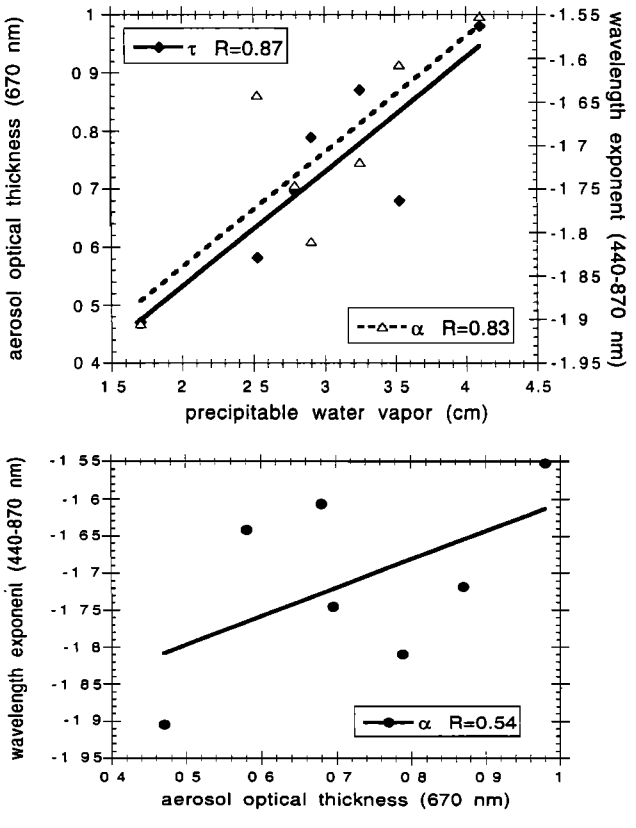

Figure 11. (top) Mean aerosol optical thickness at 670 nm (τ) and wavelength exponent ($\alpha_{870/440}$) of each air mass category as a function of the category mean precipitable water vapor P_w. (bottom) Mean wavelength exponent ($\alpha_{870/440}$) of each air mass category as a function of the category mean aerosol optical thickness. Lines are the linear regression through the data with the correlation coefficients shown. Data are given in Table 3.

separated into seven categories, depending on origin sector and height and degree of stagnation. Figure 10 shows an example from each of the categories.

The mean values of optical thickness τ, two-wavelength angström coefficient ($\alpha_{870/440}$) and precipitable water vapor P_w measured by the AERONET radiometer at Cuiabá during the study period are shown in Table 3 for each category. Note that $\alpha_{870/440}$ is defined as

$$\alpha_{870/440} = \frac{\ln(\tau_{870}/\tau_{440})}{\ln(870/440)} \quad (7)$$

which is different from the angström coefficient defined in section 4. Using a one-way classification analysis of variance and an F-test to test the statistical significance, we find that none of the categories is statistically the same in all the variables. This supports the original division of the trajectories into categories. The relationship between these variables is depicted in Figure 11. In Cuiabá, large optical thicknesses are associated with larger amounts of water vapor in the column. Likewise, high P_w are associated with less spectral dependence or larger particles. One explanation for these relationships is that very heavy smoke is not locally produced in Cuiabá but is transported from deforestation zones on the rain forest fringe. Thus high optical thicknesses are associated with transport of higher humidity air located in the rain forest. Also, smoke particles transported from forest burning are larger, corresponding to the bigger particles found in the forest model of Table 1.

The relationship between optical thickness and spectral dependence or particle size is less certain. Particle size variability can also be investigated by examining retrieved size distributions. During the analysis period, 22 almucantar inversions were recorded. These were organized by trajectory category and averaged, so that we have a mean volume size distribution representative of the category. The results are shown in Figure 12. Plotted are the retrievals of the Nakajima inversion with the correction for small particles. Lognormal parameters of the accumulation mode are given in Table 4. The coarse mode is extremely variable and optically unimportant at visible wavelengths and will be ignored. The accumulation mode shows a degree of variability unexpected from previous work in creating the smoke aerosol model.

6.2. Precipitable Water Vapor as Air Mass Tracer

The analysis of back trajectories at Cuiabá shows that some of the variability in the data may be indicative of different air masses over Brazil. Originally, we had divided the database into cerrado and forest stations in order to expose regional variations in smoke, but we found little evidence that the smoke varied significantly between the two regions. The back trajectory analysis at Cuiabá shows a different method of parameterization. Because the smoke-laden air masses in Brazil move around, a tracer needs to be identified that can be used to differentiate between air masses and thereby differentiate between smoke characteristics. Two potential variables measured by AERONET and possibly derived from remote sensing are optical thickness and precipitable water vapor. The original analysis showed that there was no systematic variation in aerosol characteristics with optical thickness. The remaining variable to investigate is precipitable water vapor.

Figure 13 shows the relationship between precipitable water vapor and aerosol optical thickness at 670 nm for the entire original database divided into cerrado and forest stations. The forest stations show virtually no relationship between the two variables, while there is a significant relationship at the cerrado stations. The forest stations have overall higher values of pre-

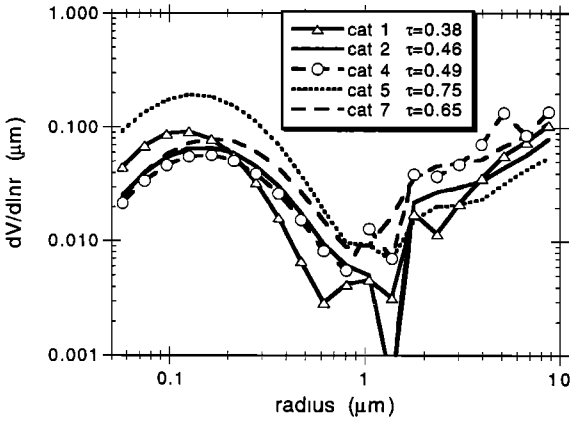

Figure 12. Mean category volume size distributions, corrected for small particles. Shown are the mean category optical thicknesses, calculated from the Sun data but measured at the time each almucantar was observed.

Table 4. Number of Almucantars, Mean Sun Optical Thickness at 670 nm at the Time of the Almucantar Measurements, and Lognormal Parameters for Mean Accumulation Mode in Each Category

Category	Retrievals	τ	V_0, μm	r_m	σ
1	6	0.38	0.09	0.118	0.60
2	3	0.46	0.06	0.152	0.70
4	7	0.49	0.07	0.152	0.70
5	2	0.75	0.19	0.135	0.70
7	2	0.65	0.08	0.170	0.70

cipitable water vapor because of the moister conditions of the adjacent rain forest. The aerosol loading has more to do with local fire counts than with variations in the already moist atmospheric column. The cerrado stations have a greater variability of precipitable water vapor, depending on air mass origin. Optical thickness in the cerrado depends on air mass origin as well as local fire counts. Moister air masses bring smokier conditions. We saw this originally in the small Cuiabá 1995 subset (Figure 11). In Figure 13 we see this generalization applies to all the cerrado sites.

Despite the suggestion that smoky air masses could be parameterized by precipitable water vapor, precipitable water vapor actually provides no advantage over optical thickness. Figure 14 shows the full database sorted by precipitable water vapor and then averaged for every 30–90 individual size distributions. The accumulation mode has been corrected at the small particle edge as in Figure 1. Because precipitable water vapor is somewhat correlated to optical thickness (Figure 13), it is also correlated to total volume in the size distributions. As P_w increases, in general, aerosol volume also increases. From the analysis with the 1995 Cuiabá data, we expected to find a shift in accumulation mode size from small particles at low values of P_w to larger particles at high values of P_w. This is not evident in the full database. In fact, there is a suggestion that the opposite may be true. Accumulation mode particle size is largest for very low values of P_w. This can be seen more clearly in Figure 15. However, the striking information of Figure 15 is not the variation in particle size at low P_w but how consistent smoke aerosol particle size can be over most of the range of P_w. Because of this consistency, there is no reason to prefer precipitable water vapor as the parameterization of smoke properties. Aerosol optical thickness remains the variable of choice due to its direct relationship to aerosol volume.

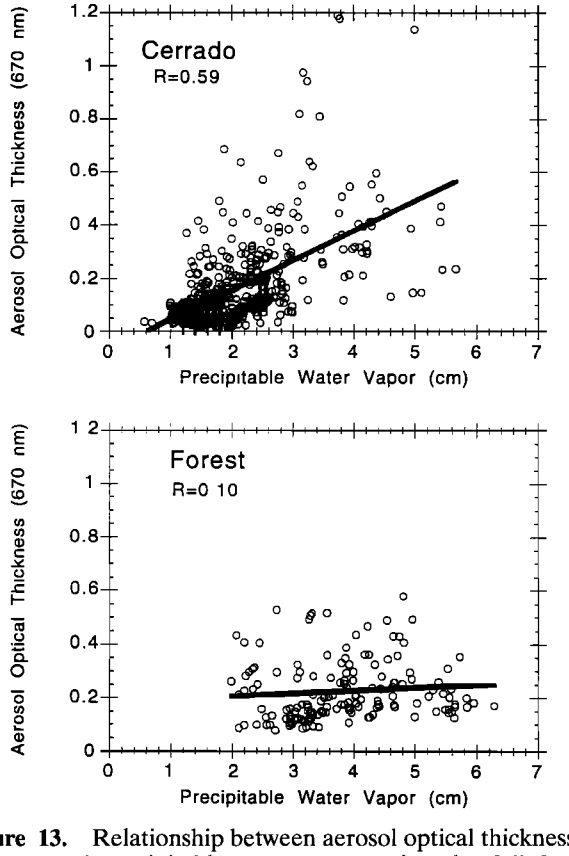

Figure 13. Relationship between aerosol optical thickness at 670 nm and precipitable water vapor using the full 3-year database collected at the cerrado stations (top) and the forest stations (bottom).

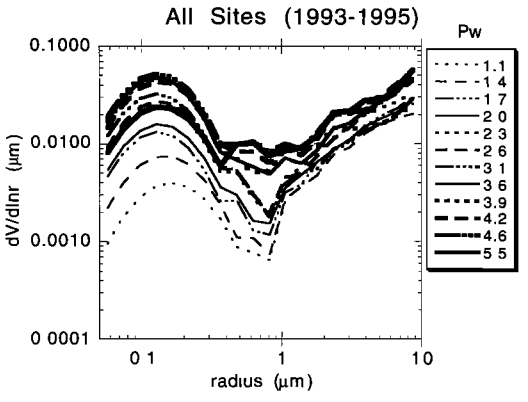

Figure 14. Volume size distributions as function of precipitable water vapor calculated from all the stations over the 3-year database (1993–1995). Each curve represents a mean of 30–90 individual volume size distribution retrievals. Size distributions are corrected at the small particle end for overprediction of volume by the inversion method.

7. Conclusions

The smoke aerosol model presented here is based on a database of over 800 volume size distributions inverted from sky radiance data measured by AERONET in Brazil over a 3-year period. The results show that the size distribution is bimodal. The accumulation mode can be represented as a lognormal with mean modal radius in the volume distribution of 0.132 ± 0.014 μm and σ = 0.60 ± 0.04. The mean characteristics of the accumulation mode remain basically the same from year to year and region to region. The properties do not systematically vary with aerosol loading or with air mass moisture. However, there is variability in the data set. At one location this variability in aerosol size distribution was associated with different air mass origins. The model was tested against independent data sets. It was able to predict backscattering path radiance and phase function correctly to within its estimated uncertainties. The largest remaining uncertainties are refractive index and single scattering albedo.

Although our database and resulting analysis does have many advantages, including a long time series, a wide spatial distribution of sites, and the measurement of undisturbed ambient aerosol of the total aerosol column, it also has inherent

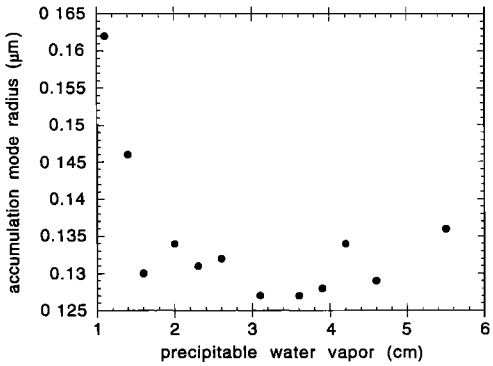

Figure 15. Modal radius of the accumulation mode calculated from the curves of Figure 14.

biases. Data are only collected during cloudless periods of homogeneous smoke. Our database does not include smoke that has recently been processed through a cloud or fresh smoke recently emitted by a fire. It tends to overemphasize data at the lower optical thicknesses because as aerosol loading increases, the tendency to encounter inhomogeneous skies also increases. Much of the heaviest smoke loading remains unaccounted for in the data set. The model was shown to accurately predict phase function of an independent data set, but this independent phase function was measured during the same homogeneous sky conditions that are well represented in our database. There remained a question of how well the model would work when applied to smoke in conditions ignored by the AERONET retrieval processes. Recently, the smoke model was incorporated in the Earth Observation System–Moderate Resolution Imaging Spectroradiometer (EOS-MODIS) aerosol retrieval software and applied to high-altitude remote sensing data over the Amazon Basin [*Chu et al.*, this issue]. The analysis included several retrievals of extremely high aerosol loading, well beyond the range used in the derivation of the model. The retrievals, dependent on the model-predicted phase function, produce results that agree well with simultaneous data measured on the ground with sunphotometers. These results are encouraging and suggest that the smoke aerosol model is sufficiently robust to be used in the EOS-MODIS operational global retrieval of aerosol optical depth [*Kaufman et al.*, 1997] and in climate models as well.

Acknowledgments. We would like to thank V. W. J. H. Kirchhoff and the many scientists and technicians of the Instituto Nacional de Pesquisas Espaciais (INPE) for their collaboration and support during the 3 years of data collection in Brazil, culminating with SCAR-B. We would also like to acknowledge the AERONET team of Thomas Eck, Wayne Newcomb, Ilya Slutsker, and Ross Nelson for instrument deployment, maintainence, calibration, and quality control. Thanks also go to Jeffrey Reid, Qiang Ji, and an anonymous reviewer for many helpful comments.

References

Anderson, B. E., W. B. Grant, G. L. Gregory, E. V. Browell, J. E. Collins, G. W. Sachse, D. R. Bagwell, C. H. Hudgins, D. R. Blake, and N. J. Blake, Aerosols from biomass burning over the tropical South Atlantic region: Distributions and impacts, *J. Geophys. Res.*, *101*, 24,117–24,138, 1996.

Andreae, M. O., B. E. Anderson, D. R. Blake, J. D. Bradshaw, J. E. Collins, G. L. Gregory, G. W. Sachse, and M. C. Shipham, Influence of plumes from biomass burning on atmospheric chemistry over the equatorial and tropical South Atlantic during CITE 3, *J. Geophys. Res.*, *99*, 12,793–12,808, 1994.

Andreae, M. O., E. Atlas, H. Cachier, W. R. Cofer, III, G. W. Harris, G. Helas, R. Koppmann, J.-P. Lacaux, and D. E. Ward, Trace gas and aerosol emissions from savanna fires, in *Biomass Burning and Global Change*, edited by J. S. Levine, pp. 278–295, MIT Press, Cambridge, Mass., 1996.

Chu, D. A., Y. J. Kaufman, L. A. Remer, and B. N. Holben, Remote sensing of smoke from MODIS airborne simulator during the SCAR-B experiment, *J. Geophys. Res.*, this issue.

Dave, J. V., and J. Gazdag, A modified Fourier transform method for multiple scattering calculations in a plane parallel Mie atmosphere, *Appl. Opt.*, *9*, 1457–1466, 1970.

Eck, T., B. N. Holben, I. Slutsker, and A. Setzer, Measurements of irradiance attenuation and estimation of aerosol single scattering albedo for biomass burning aerosols in Amazonia, *J. Geophys. Res.*, this issue.

Ferrare, R. A., R. S. Fraser, and Y. J. Kaufman, Satellite measurements of large-scale air pollution: Measurements of forest fire smoke, *J. Geophys. Res.*, *95*, 9911–9925, 1990.

Folkins, I., R. Chatfield, D. Baumgardner, and M. Proffitt, Biomass burning and deep convection in southeastern Asia: Results from ASHOE/MAESA, *J. Geophys. Res.*, *102*, 13,291–13,299, 1997.

Herman, J. R., P. K. Bhartia, O. Torres, C. Hsu, C. Seftor, and E. Celarier, Global distribution of UV-absorbing aerosols from Nimbus 7/TOMS data, *J. Geophys. Res.*, *102*, 16,911–16,922, 1997.

Hobbs, P. V., and L. F. Radke, Cloud condensation nuclei from a simulated forest fire, *Science*, *163*, 279–280, 1969.

Hobbs, P. V., J. S. Reid, R. A. Kotchenruther, R. J. Ferek, and R. Weiss, Direct radiative forcing by smoke from biomass burning, *Science*, *275*, 1776–1778, 1997.

Holben, B. N., A. Setzer, T. F. Eck, A. Pereira, and I. Slutsker, Effect of dry season biomass burning on Amazon basin aerosol concentrations and optical properties, *J. Geophys. Res.*, *101*, 19,455–19,464, 1996a.

Holben, B. N., D. Tanré, Y. J. Kaufman, I. Slutsker, and D. E. Ward, Single-scattering albedo approximated from ground based measurements of aerosol optical thickness in the Amazon Basin in *Smoke, Clouds, and Radiation–Brazil: Proceedings*, edited by V. W. J. H. Kirchhoff, pp. 73–78, Transtec Editorial, Sao Jose dos Campos, Brazil, 1996b.

Holben, B. N., et al., Automatic sun and sky scanning radiometer system for network aerosol monitoring, *Remote Sens. Environ.*, in press, 1998.

Hoppel, W. A., J. W. Fitzgerald, G. M. Frick, R. E. Larson, and E. J. Mack, Aerosol size distributions and optical properties found in the marine boundary layer over the Atlantic Ocean, *J. Geophys. Res.*, *95*, 3659–3686, 1990.

Hudson, J. G., J. Hallett, and C. F. Rogers, Field and laboratory measurements of cloud-forming properties of combustion aerosols, *J. Geophys. Res.*, *96*, 10,847–10,859, 1991.

Huebert, B. J., G. Lee, and W. L. Warren, Airborne aerosol inlet passing efficiency measurement, *J. Geophys. Res.*, *95*, 16,369–16,381, 1990.

Intergovernmental Panel on Climate Change (IPCC), Radiative forcing of climate change, in *Climate Change 1996*, 339 pp., World Meteorol. Organ., Geneva, 1996.

Ji, Q., S.-C. Tsay, Y. J. Kaufman and G. E. Shaw, SCAR-B ground-based measurements of aerosol microphysics in Cuiabá, in *Smoke, Clouds, and Radiation–Brazil: Proceedings*, edited by V. W. J. H. Kirchhoff, pp. 79–83, Transtec Editorial, Sao Jose dos Campos, Brazil, 1996.

Kaufman, Y. J., and R. S. Fraser, The effect of smoke particles on clouds and climate forcing, *Science*, *277*, 1636–1639, 1997.

Kaufman, Y. J., and B. N. Holben, Hemispherical backscattering by biomass burning and sulfate particles derived from sky measurements, *J. Geophys. Res.*, *101*, 19,433–19,445, 1996.

Kaufman, Y. J., and T. Nakajima, Effect of Amazon smoke on cloud microphysics and albedo—Analysis from satellite imagery, *J. Appl. Meteorol.*, *32*, 729–744, 1993.

Kaufman, Y. J., and D. Tanré, Effect of variations in supersaturation on the formation of cloud condensation nuclei, *Nature*, *369*, 45–48, 1994.

Kaufman, Y. J., A. Setzer, D. Ward, D. Tanré, B. N. Holben, P. Menzel, M. C. Pereira, and R. Rasmussen, Biomass Burning Air-

borne and Spaceborne Experiment in the Amazonas (BASE-A), *J. Geophys. Res.*, *97*, 14,581–14,599, 1992.

Kaufman, Y. J., A. Gitelson, A. Karnieli, E. Ganor, R. S. Fraser, T. Nakajima, S. Mattoo, and B. N. Holben, Size distribution and scattering phase function of aerosol particles retrieved from sky brightness measurements, *J. Geophys. Res.*, *99*, 10,341–10,356, 1994.

Kaufman, Y. J., D. Tanré, L. A. Remer, E. Vermote, A. Chu, and B. N. Holben, Remote sensing of tropospheric aerosol from EOS-MODIS over the land using dark targets and dynamic aerosol models, *J. Geophys. Res.*, *102*, 17,051–17,067, 1997.

Kaufman, Y. J., et al., Smoke, clouds, and radiation-Brazil (SCAR-B) experiment, *J. Geophys. Res.*, this issue.

Kotchenruther, R. A., and P. V. Hobbs, Humidification factors of aerosols from biomass burning in Brazil, *J. Geophys. Res.*, this issue.

Le Canut, P., M. O. Andreae, G. W. Harris, F. G. Wienhold, and T. Zenker, Aerosol optical properties over southern Africa during SAFARI-92, in *Biomass Burning and Global Change*, edited by J. S. Levine, pp. 441–459, MIT Press, Cambridge, Mass., 1996a.

Le Canut, P., M. O. Andreae, G. W. Harris, F. G. Wienhold, and T. Zenker, Airborne studies of emissions from savanna fires in southern Africa, 1, Aerosol emissions measured with a laser particle counter, *J. Geophys. Res.*, *101*, 23,615–23,630, 1996b.

Lenoble, J., and C. Brogniez, A comparative review of radiation aerosol models, *Beitr. Phys. Atmos.*, *57*, 1–20, 1984.

Maenhaut, W., G. Koppen, and P. Artaxo, Long-term atmospheric aerosol study in Cuiabá, Brazil: Multielemental composition, sources, and impact of biomass burning, in *Biomass Burning and Global Change*, edited by J. S. Levine, pp. 637–652, MIT Press, Cambridge, Mass., 1996.

Martins, J. V., P. Artaxo, P. V. Hobbs, C. Liousse, H. Cachier, Y. J. Kaufman, and A. Plana-Fattori, Particle-size distributions, elemental composition, carbon measurements, and optical properties of smoke from biomass burning in the Pacific Northwest of the United States, in *Biomass Burning and Global Change*, edited by J. S. Levine, pp. 716–732, MIT Press, Cambridge, Mass., 1996.

Martins, J. V., P. V. Hobbs, R. E. Weiss, and P. Artaxo, Sphericity and morphology of smoke particles from biomass burning in Brazil, *J. Geophys. Res.*, this issue.

Nakajima, T., M. Tanaka, and T. Yamauchi, Retrieval of the optical properties of aerosols from aereole and extinction data., *Appl. Opt.*, *22*, 2951–2959, 1983.

Nakajima, T., M. Takamura, M. Yamano, M. Shiobara, T. Yamauchi, R. Goto, and K. Murai, Consistency of aerosol size distribution inferred from measurements of solar radiation and aureole, *J. Meteorol. Soc. Jpn.*, *64*, 765–776, 1986.

Penner, J. E., R. E. Dickinson, and C. A. O'Neill, Effects of aerosol from biomass burning on the global radiation budget, *Science*, *256*, 1432–1434, 1992.

Pickering, K. E., A. M. Thompson, D. P. McNamara, M. R. Schoeberl, H. E. Fuelberg, R. O. L. Jr., M. V. Watson, K. Fakhruzzaman, and A. S. Bachmeier, TRACE-A trajectory intercomparison, 1, Effects of different input analyses, *J. Geophys. Res.*, *101*, 23,909–23,925, 1996.

Prins, E. M., J. M. Feltz, W. P. Menzel, and D. E. Ward, An overview of GOES 8 diurnal fire and smoke results for SCAR-B and the 1995 fire season in South America, *J. Geophys. Res.*, this issue.

Radke, L. F., D. A. Hegg, P. V. Hobbs, J. D. Nance, J. H. Lyons, K. K. Laursen, P. J. Reagan, and D. E. Ward, Particulate and trace gas emission from large biomass fires in North America, in *Global Biomass Burning: Atmospheric, Climatic, and Biospheric Implications*, edited by J. S. Levine, pp. 209–224, MIT Press, Cambridge, Mass., 1991.

Reid, J. S., and P. V. Hobbs, Physical and optical properties of young smoke from individual biomass fires in Brazil, *J. Geophys. Res.*, this issue.

Reid, J. S., P. V. Hobbs, R. J. Ferek, D. R. Blake, J. V. Martins, M. R. Dunlap, and C. Liousse, Physical, chemical and optical properties of regional hazes dominated by smoke in Brazil, *J. Geophys. Res.*, this issue.

Remer, L. A., and Y. J. Kaufman, Dynamical aerosol model: Urban/industrial aerosol, *J. Geophys. Res.*, *103*, 13,859–13,871, 1998.

Remer, L. A., Y. J. Kaufman, and B. N. Holben, The size distribution of ambient aerosol particles: Smoke versus urban/industrial aerosol, in *Biomass Burning and Global Change*, edited by J. S. Levine, pp. 519–530, MIT Press, Cambridge, Mass., 1996.

Remer, L. A., S. Gassó, D. A. Hegg, Y. J. Kaufman, and B. N. Holben, Urban/industrial aerosol: Ground-based sun/sky radiometer and airborne in situ measurements, *J. Geophys Res.*, *102*, 16,849–16,859, 1997.

Rodgers, C. F., J. G. Hudson, B. Zielinska, R. L. Tanner, J. Hallett, and J. G. Watson, Cloud condensation nuclei from biomass burning, in *Global Biomass Burning: Atmospheric, Climatic, and Biospheric Implications*, edited by J. S. Levine, pp. 431–438, MIT Press, Cambridge, Mass., 1991.

Ross, J. L., and P. V. Hobbs, Radiative characteristics of regional hazes dominated by smoke from biomass burning in Brazil: Closure tests and direct radiative forcing, *J. Geophys. Res.*, this issue.

Schoeberl, M. R., and L. C. Sparling, Trajectoring modeling, in *Diagnostic Tools in Atmospheric Science, Proceedings*, edited by G. Visconti, pp. 289–305, Int. Sch. of Phys., Enrico Fermi, 1995.

Schoeberl, M. R., S. D. Doiron, L. R. Lait, P. A. Newman, and A. J. Krueger, A simulation of the Cerro Hudson SO_2 cloud, *J. Geophys. Res.*, *98*, 2949–2956, 1993.

Shettle, E. P., and R. W. Fenn, Models for the aerosol of the lower atmosphere and the effect of humidity variations on their optical properties, *AFGL Tech. Rep.*, *TR-79-0214*, 1979.

Stocks, B. J., J. D. R. Cahoon, I. W. R. Cofer, and J. S. Levine, Monitoring large-scale forest fire behavior in northeastern Siberia using NOAA-AVHRR satellite imagery, in *Biomass Burning and Global Change*, edited by J. S. Levine, pp. 802–807, MIT Press, Cambridge, Mass., 1996.

Twomey, S. A., *Atmospheric Aerosol*, 302 pp., Elsevier Sci., New York, 1977a.

Twomey, S. A., The influence of pollution on the shortwave albedo of clouds, *J. Atmos. Sci.*, *34*, 1149–1152, 1977b.

Twomey, S. A., M. Piepgrass, and T. L. Wolfe, An assessment of the impact of pollution on global cloud albedo, *Tellus*, *36B*, 356–366, 1984.

Wiscombe, W. J., and G. W. Grams, The backscatter fraction in two stream approximations, *J. Atmos. Sci.*, *33*, 2440–2451, 1976.

Yamasoe, M. A., Y. J. Kaufman, O. Dubovik, L. A. Remer, B. N. Holben, and P. Artaxo, Retrieval of the real part of the refractive index of smoke particles from Sun/sky measurements during SCAR-B, *J. Geophys. Res.*, this issue.

B. N. Holben, Laboratory for Terrestrial Physics, 923, NASA Goddard Space Flight Center, Greenbelt, MD 20771.

Y. J. Kaufman and L. A. Remer, Laboratory for Atmospheres, 913, NASA Goddard Space Flight Center, Greenbelt, MD 20771. (e-mail: remer@climate.gsfc.nasa.gov)

D. McNamara and A. M. Thompson, Laboratory for Atmospheres, 916, NASA Goddard Space Flight Center, Greenbelt, MD 20771.

(Received August 29, 1997; revised November 25, 1997; accepted January 15, 1998.)